Structure of pressure-gradient-driven current singularity in ideal magnetohydrodynamic equilibrium

OPEN ACCESS
IOP Publishing
Plasma Physics and Controlled Fusion
Plasma Phys. Control. Fusion **65** (2023) 129601 (1p)
https://doi.org/10.1088/1361-6587/ad0852

Erratum: Structure of pressure-gradient-driven current singularity in ideal magnetohydrodynamic equilibrium (2023 *Plasma Phys. Controlled Fusion* **65** 034008)

Yi-Min Huang[1,*], **Yao Zhou**[2], **Joaquim Loizu**[3], **Stuart Hudson**[4] and **Amitava Bhattacharjee**[1]

[1] Department of Astrophysical Sciences and Princeton Plasma Physics Laboratory, Princeton, NJ 08543, United States of America
[2] Institute of Natural Sciences, School of Physics and Astronomy, and MOE-LSC, Shanghai Jiao Tong University, Shanghai 200240, People's Republic of China
[3] École Polytechnique Fédérale de Lausanne, Swiss Plasma Center, CH-1015 Lausanne, Switzerland
[4] Princeton Plasma Physics Laboratory, Princeton, NJ 08543, United States of America

E-mail: yiminh@princeton.edu

Received 26 October 2023
Accepted for publication 31 October 2023

The paragraph starting at the end of page 6 in the original article should read:

Finally, we use the relation (51) to eliminate c_2 in the boundary condition (31), yielding an equation for c_1:

$$7k^2\cosh(ka)\,c_1^2 - 24\sinh(ka)\,c_1 + 24\delta a = 0. \tag{52}$$

The solution is

$$c_1 = \frac{12\sinh(ka) - \sqrt{144\sinh^2(ka) - 168a\delta k^2\cosh(ka)}}{7k^2\cosh(ka)}. \tag{53}$$

Here, the sign for the square root in (53) is chosen such that $c_1 \simeq a\delta/\sinh(ka)$ in the limit of a small perturbation.

These errors had no impact on the remaining part of the original article.

* Author to whom any correspondence should be addressed.

ORCID iDs

Yi-Min Huang https://orcid.org/0000-0002-4237-2211
Yao Zhou https://orcid.org/0000-0002-3616-2912
Stuart Hudson https://orcid.org/0000-0003-1530-2733
Amitava Bhattacharjee https://orcid.org/0000-0001-6411-0178

OPEN ACCESS
IOP Publishing
Plasma Physics and Controlled Fusion
Plasma Phys. Control. Fusion **65** (2023) 034008 (12pp)
https://doi.org/10.1088/1361-6587/acb382

Structure of pressure-gradient-driven current singularity in ideal magnetohydrodynamic equilibrium

Yi-Min Huang[1,*], Yao Zhou[2], Joaquim Loizu[3], Stuart Hudson[4] and Amitava Bhattacharjee[1]

[1] Department of Astrophysical Sciences and Princeton Plasma Physics Laboratory, Princeton University, Princeton, NJ 08543, United States of America
[2] School of Physics and Astronomy, Institute of Natural Sciences, and MOE-LSC, Shanghai Jiao Tong University, Shanghai 200240, People's Republic of China
[3] École Polytechnique Fédérale de Lausanne, Swiss Plasma Center, CH-1015 Lausanne, Switzerland
[4] Princeton Plasma Physics Laboratory, Princeton University, Princeton, NJ 08543, United States of America

E-mail: yiminh@princeton.edu

Received 29 November 2022
Accepted for publication 16 January 2023
Published 16 February 2023

Abstract

Singular currents typically appear on rational surfaces in non-axisymmetric ideal magnetohydrodynamic (MHD) equilibria with a continuum of nested flux surfaces and a continuous rotational transition. These currents have two components: a surface current (Dirac δ-function in flux surface labeling) that prevents the formation of magnetic islands, and an algebraically divergent Pfirsch–Schlüter current density when a pressure gradient is present across the rational surface. On flux surfaces adjacent to the rational surface, the traditional treatment gives the Pfirsch–Schlüter current density scaling as $J \sim 1/\Delta\iota$, where $\Delta\iota$ is the difference of the rotational transform relative to the rational surface. If the distance s between flux surfaces is proportional to $\Delta\iota$, the scaling relation $J \sim 1/\Delta\iota \sim 1/s$ will lead to a paradox that the Pfirsch–Schlüter current is not integrable. In this work, we investigate this issue by considering the pressure-gradient-driven singular current in the Hahm–Kulsrud–Taylor problem, which is a prototype for singular currents arising from resonant magnetic perturbations. We show that not only the Pfirsch–Schlüter current density but also the diamagnetic current density are divergent as $\sim 1/\Delta\iota$. However, due to the formation of a Dirac δ-function current sheet at the rational surface, the neighboring flux surfaces are strongly packed with $s \sim (\Delta\iota)^2$. Consequently, the singular current density $J \sim 1/\sqrt{s}$, making the total current finite, thus resolving the paradox. Furthermore, the strong packing of flux surfaces causes a steepening of the pressure gradient near the rational surface, with $\nabla p \sim \mathrm{d}p/\mathrm{d}s \sim 1/\sqrt{s}$. In general non-axisymmetric MHD equilibrium, contrary to Grad's conjecture that the pressure profile is flat around densely distributed rational surfaces, our result suggests a pressure profile that densely steepens around them.

* Author to whom any correspondence should be addressed.

Keywords: current singularity, asymptotic analysis, boundary layer, magnetohydrodynamic equilibrium, resonant magnetic perturbation

(Some figures may appear in colour only in the online journal)

1. Introduction

Magnetic field configurations with nested flux surfaces are desirable for plasma confinement fusion devices, due to the much faster motion of charged particles along the magnetic field lines than in transverse directions. Fusion devices with nested flux surfaces effectively insulate hot plasmas from device walls, facilitating good confinement. Axisymmetric fusion devices, such as tokamaks, can have a continuum of nested flux surfaces. However, for devices that are inherently three-dimensional (3D), such as stellarators [1–4], the existence of a continuum of nested flux surfaces is not guaranteed.

Nevertheless, many existing magnetohydrodynamic (MHD) equilibrium solvers for stellarators, e.g. VMEC [5], NSTAB [6, 7], and DESC [8], assume a continuum of nested flux surfaces as a point of departure. These solvers seek equilibria satisfying the MHD force balance equation

$$-\nabla p+\boldsymbol{J}\times\boldsymbol{B}=0 \tag{1}$$

either by minimizing the MHD potential energy (i.e. the sum of the magnetic and thermal energies) or by directly imposing the force balance as a constraint. Here, p, $\boldsymbol{B}$, and $\boldsymbol{J}=\nabla\times\boldsymbol{B}$ are standard notations for the plasma pressure, the magnetic field, and the current density.

Toroidal 3D MHD equilibria with a continuum of nested flux surfaces can potentially give rise to current singularities at rational surfaces, where magnetic field lines form closed loops rather than fill the flux surfaces ergodically. To understand this issue, note that the force balance equation (1) implies that the component of the current density perpendicular to the magnetic field is given by

$$\boldsymbol{J}_\perp=\frac{\boldsymbol{B}\times\nabla p}{B^2}. \tag{2}$$

By writing

$$\boldsymbol{J}=\frac{J_\parallel}{B}\boldsymbol{B}+\boldsymbol{J}_\perp, \tag{3}$$

the condition $\nabla\cdot\boldsymbol{J}=0$ implies

$$\boldsymbol{B}\cdot\nabla\frac{J_\parallel}{B}=-\nabla\cdot\boldsymbol{J}_\perp=-\left(\boldsymbol{B}\times\nabla p\right)\cdot\nabla\frac{1}{B^2}, \tag{4}$$

and in general $\nabla\cdot\boldsymbol{J}_\perp\neq0$ if $\nabla p\neq0$. In a straight-field-line coordinate system (Ψ,θ,φ), the magnetic field is given by

$$\boldsymbol{B}=\nabla\Psi\times\left(\nabla\theta-\iota\nabla\varphi\right),$$

where Ψ is the toroidal flux function, θ is a poloidal angle, φ is a toroidal angle, and $\iota=\iota\left(\Psi\right)$ is the rotational transform. In these coordinates, the magnetic differential operator $\boldsymbol{B}\cdot\nabla$ is given by

$$\boldsymbol{B}\cdot\nabla f=\frac{1}{\mathcal{J}}\left(\frac{\partial f}{\partial\varphi}+\iota\frac{\partial f}{\partial\theta}\right), \tag{5}$$

where $\mathcal{J}$ is the Jacobian of the coordinates. By using Fourier representations

$$J_\parallel/B=\sum_{m,n}u_{mn}\left(\Psi\right)\exp\left[i\left(m\theta-n\varphi\right)\right] \tag{6}$$

and

$$\mathcal{J}\nabla\cdot\boldsymbol{J}_\perp=\sum_{m,n}h_{mn}\left(\Psi\right)\exp\left[i\left(m\theta-n\varphi\right)\right], \tag{7}$$

the magnetic differential equation (4) can be written as

$$\sum_{m,n}i\left(\iota\left(\Psi\right)m-n\right)u_{mn}\left(\Psi\right)\exp\left[i\left(m\theta-n\varphi\right)\right]=-\sum_{m,n}h_{mn}\left(\Psi\right)\exp\left[i\left(m\theta-n\varphi\right)\right]. \tag{8}$$

Therefore, $J_\parallel/B$ can be expressed as

$$J_\parallel/B=\sum_{m,n\neq0,0}\left[i\frac{h_{mn}\left(\Psi\right)}{\iota\left(\Psi\right)m-n}+\Delta_{mn}\delta\left(\iota\left(\Psi\right)m-n\right)\right]\times\exp\left[i\left(m\theta-n\varphi\right)\right]+u_{00}\left(\Psi\right), \tag{9}$$

where u_{00} is a flux function and Δ_{mn} are coefficients to be determined [9, 10].

Equation (9) exhibits two types of singularities at rational surfaces, where the rotational transform ι is rational numbers. Let $x=\iota\left(\Psi\right)m-n$. The first term in equation (9), known as the Pfirsch–Schlüter current, has a $1/x$-type singularity at the rational surface with $\iota=n/m$. The second term is a Dirac δ-function singularity, which is permitted because $x\delta(x)=0$.

The physical quantity associated with the current density is the total current through a surface. The Dirac δ-function type singularities are sheet currents at rational surfaces. Even though the current density becomes infinite, the total current is finite because the Dirac δ function is integrable. The $1/x$-type singularities of the Pfirsch–Schlüter current poses a more serious problem. If the distance between the rational surface and neighboring flux surfaces is proportional to x, then the total current through a constant-φ surface element enclosed by θ, $\theta+\mathrm{d}\theta$, $x=\epsilon_1$, and $x=\epsilon_2$ is proportional to $\int_{\epsilon_1}^{\epsilon_2}\mathrm{d}x'/x'$, which diverges logarithmically when $\epsilon_1\to0$. For this reason, the $1/x$-type singularities are considered unphysical and should be avoided.

The $1/x$-type singularities can be eliminated if the plasma pressure is globally flat, but that is not of interest to magnetic confinement fusion. Grad noted that magnetically confined MHD equilibrium solutions may be constructed by considering pressure profiles that are flat in a small neighborhood of each rational surface. However, if the rotational transform $\iota(\psi)$ is continuous, the magnetic differential equation (4) is densely singular and there will be infinitely many flat-pressure regions throughout the entire plasma volume. Grad described such a pressure distribution as pathological [11]. Along this line of thought, Hudson and Kraus constructed fractal-like pressure profiles with gradients localized to where the rotational transformations are sufficiently irrational, i.e. those that satisfy a Diophantine condition [12, 13]. Alternatively, one may allow the rotational transform ι to have discontinuities such that rational surfaces do not exist.

The central difficulty associated with the $1/x$-type singularities is that they appear to give rise to divergent currents. However, this conclusion is obtained through heuristic arguments as we have discussed above rather than through a rigorous mathematical proof. The primary objective of this work is to reassess this conclusion through a simple model problem—the Hahm–Kulsrud–Taylor (HKT) problem [14, 15]. The HKT problem was originally posed as a forced reconnection problem, but in the ideal MHD limit, it also serves as a prototype for the current singularity formation driven by resonant magnetic perturbations [16]. The HKT problem is amenable to analytic solutions [17, 18] and has been studied with various numerical codes including a Grad–Shafranov (GS) solver [19], a fully Lagrangian code [20], and the Stepped Pressure Equilibrium Code (SPEC) [21] for the case with $p=0$ [16–18, 22]. In this study, we extend the established analytic and numerical solutions to include a non-vanishing pressure gradient.

This paper is organized as follows. Section 2 lays out the GS formulation of the HKT problem and provides an asymptotic analytic solution. Section 3 compares the analytic solution with numerical solutions. We conclude and discuss the future outlook in section 4.

2. GS solution of the HKT problem with pressure gradient

2.1. GS formulation for the HKT problem

The HKT problem, illustrated in figure 1, has a magnetized plasma enclosed by two conducting walls in slab geometry. Before the conducting walls are perturbed, the initial magnetic field is a smooth function of space in the domain with $-a \leqslant x \leqslant a$ and $0 \leqslant y \leqslant L$. The in-plane component points in the y direction with $B_{y0} = x$; together with a non-uniform B_{z0} component and the pressure p_0, the system is in force balance; i.e. the equation

$$\frac{B_{y0}^2 + B_{z0}^2}{2} + p_0 = \text{const} \tag{10}$$

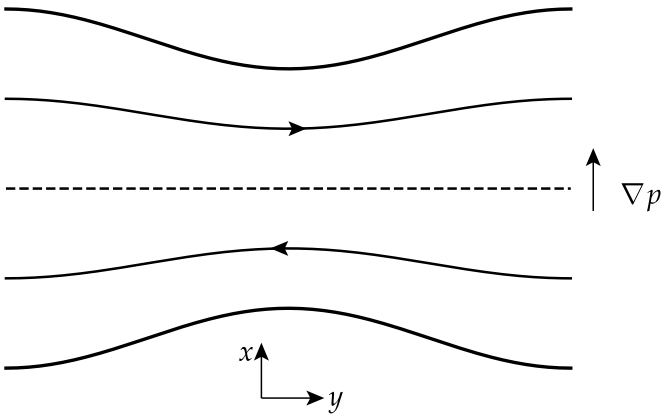

Figure 1. The Hahm–Kulsrud–Taylor problem with a pressure gradient. The in-plane components of the magnetic field reverse directions at the mid-plane (the dashed line). The upper and lower boundaries are shaped by mirror-symmetric sinusoidal perturbations. In response to the perturbation, a δ-function singular current sheet develops in the mid-plane, which resonates with the boundary perturbations. The pressure gradient of the plasma drives the Pfirsch–Schlüter current density, which diverges algebraically near the resonant surface.

is satisfied. Assuming a periodic boundary condition along the y direction, we then impose a sinusoidal perturbation with an up-down symmetry that displaces the conducting walls at $x = \pm a$ to $x = \pm(a + \delta\cos(ky))$, where $k = 2\pi/L$ is the wavenumber. As the system evolves to a new equilibrium subject to the ideal MHD constraint, current singularities, including a Dirac δ-function current sheet and a pressure-gradient-driven current singularity, will develop at and around the resonant surface $x = 0$ (the dashed line in figure 1).

In response to the boundary perturbation, the flux surfaces adjust their geometries while preserving the magnetic fluxes between them in accordance with the ideal MHD constraints. The new MHD equilibrium satisfies the GS equation in Cartesian geometry

$$\nabla^2\psi = -\frac{\mathrm{d}P}{\mathrm{d}\psi}, \tag{11}$$

where

$$P = p + \frac{B_z^2}{2}. \tag{12}$$

Here, the magnetic field in Cartesian geometry, with z being the direction of translational symmetry, is expressed in terms of the poloidal (in-plane) flux function ψ as

$$\boldsymbol{B} = B_z\hat{\boldsymbol{z}} + \hat{\boldsymbol{z}} \times \nabla\psi. \tag{13}$$

In an equilibrium state both the out-of-plane component B_z and the plasma pressure p are functions of ψ.

Since the magnetic fluxes are conserved, the magnetic field is determined by the geometry of the flux surfaces. To describe the geometry of flux surfaces, we first need to choose a variable to label them. Let x_0 be the positions of flux surfaces along the

x direction before the boundary perturbation is imposed. The initial condition $B_{y0} = x_0$ yields the poloidal (in-plane) magnetic flux function $\psi(x_0) = x_0^2/2$. While it is customary in toroidal confinement devices to label flux surfaces by the magnetic flux function, for the HKT problem it is convenient to label the flux surfaces with their initial positions x_0 because a single value of ψ can correspond to more than one flux surface.

With this labeling, the geometry of flux surfaces is described by a mapping from (x_0, y) to (x, y) via a function $x(x_0, y)$. Using the chain rule, we can express the partial derivatives with respect to the Cartesian coordinates in terms of the partial derivatives of the coordinates (x_0, y):

$$\left(\frac{\partial}{\partial x}\right)_y = \frac{1}{\partial x/\partial x_0}\frac{\partial}{\partial x_0}, \tag{14}$$

$$\left(\frac{\partial}{\partial y}\right)_x = \frac{\partial}{\partial y} - \frac{\partial x/\partial y}{\partial x/\partial x_0}\frac{\partial}{\partial x_0}. \tag{15}$$

Here, the subscripts of the partial derivatives on the left-hand side indicate the coordinates that are fixed; the partial derivatives on the right-hand side are with respect to the (x_0, y) coordinates. Hereafter, partial derivatives are taken to be with respect to the (x_0, y) coordinates by default, unless otherwise indicated by the subscripts.

Using these relations for partial derivatives, the Cartesian components of the in-plane magnetic field are given by

$$B_x = -\left(\frac{\partial\psi}{\partial y}\right)_x = \frac{\partial x/\partial y}{\partial x/\partial x_0}\frac{\mathrm{d}\psi}{\mathrm{d}x_0} \tag{16}$$

and

$$B_y = \left(\frac{\partial\psi}{\partial x}\right)_y = \frac{1}{\partial x/\partial x_0}\frac{\mathrm{d}\psi}{\mathrm{d}x_0}. \tag{17}$$

The out-of-plane component B_z is determined by the conservation of the out-of-plane magnetic flux as

$$B_z(x_0) = \frac{B_{z0}(x_0)}{\left\langle \frac{\partial x}{\partial x_0}\right\rangle}. \tag{18}$$

Here, B_{z0} is the initial z-component of the magnetic field and the flux surface average $\langle f\rangle$ is defined as

$$\langle f\rangle \equiv \frac{1}{L}\int_0^L f(x_0, y)\,\mathrm{d}y \tag{19}$$

for an arbitrary function $f(x_0, y)$, where L is the period of the system along the y direction. Likewise, the pressure is determined by the adiabatic energy equation as

$$p(x_0) = \frac{p_0(x_0)}{\left\langle \frac{\partial x}{\partial x_0}\right\rangle^{\gamma}}, \tag{20}$$

where $p_0(x_0)$ is the initial pressure profile and γ is the adiabatic index.

From the relation $\boldsymbol{J} = \nabla\times\boldsymbol{B}$, the out-of-plane component of the current density is given by

$$J_z = \nabla^2\psi = \left(\frac{\mathrm{d}\psi}{\mathrm{d}x_0}\right)^{-1}\frac{\partial}{\partial x_0}\left(\frac{B_x^2 + B_y^2}{2}\right) - \frac{\partial B_x}{\partial y} \tag{21}$$

and the poloidal (in-plane) component $\boldsymbol{J}_p$ is

$$\boldsymbol{J}_p = \frac{\mathrm{d}B_z}{\mathrm{d}\psi}\nabla\psi\times\hat{\boldsymbol{z}} = -\frac{\mathrm{d}B_z}{\mathrm{d}\psi}\boldsymbol{B}_p, \tag{22}$$

where $\boldsymbol{B}_p = \hat{\boldsymbol{z}}\times\nabla\psi$ is the poloidal (in-plane) component of the magnetic field. Substituting equation (21) in equation (11), the GS equation can be written as

$$-\frac{\partial}{\partial x_0}\left(\frac{B_x^2 + B_y^2}{2} + P\right) + \frac{\partial B_x}{\partial y}\frac{\mathrm{d}\psi}{\mathrm{d}x_0} = 0. \tag{23}$$

2.2. Outer-region solution

For a small boundary perturbation, we may linearize the GS equation in terms of the displacements of the flux surfaces along the x direction $\xi(x_0, y) \equiv x(x_0, y) - x_0$. To the leading order of ξ, the magnetic field components are

$$B_x \simeq \frac{\partial\xi}{\partial y}\frac{\mathrm{d}\psi}{\mathrm{d}x_0}, \tag{24}$$

$$B_y \simeq (1 - \partial\xi/\partial x_0)\frac{\mathrm{d}\psi}{\mathrm{d}x_0}, \tag{25}$$

and

$$B_z \simeq B_{z0}(x_0)\left(1 - \left\langle\frac{\partial\xi}{\partial x_0}\right\rangle\right). \tag{26}$$

The linearized pressure is

$$p \simeq p_0(x_0)\left(1 - \gamma\left\langle\frac{\partial\xi}{\partial x_0}\right\rangle\right). \tag{27}$$

Using equations (24)–(27), and the relation $\psi = x_0^2/2$ in equation (23), the linearized GS equation now reads

$$\frac{\partial}{\partial x_0}\left(x_0^2\frac{\partial\xi}{\partial x_0} + \left(B_{z0}^2 + p_0\gamma\right)\left\langle\frac{\partial\xi}{\partial x_0}\right\rangle\right) + x_0^2\frac{\partial^2\xi}{\partial y^2} = 0. \tag{28}$$

If we adopt the ansatz $\xi = \bar{\xi}(x_0)\cos(ky)$, then $\langle\partial\xi/\partial x_0\rangle = 0$ and the linearized GS equation reduces to

$$\frac{\mathrm{d}^2}{\mathrm{d}x_0^2}\left(x_0\bar{\xi}\right) - k^2 x_0\bar{\xi} = 0. \tag{29}$$

The general solution of equation (29) is a linear superposition of two independent solutions

$$\bar{\xi} = c_1\frac{\sinh(k|x_0|)}{x_0} + c_2\frac{\cosh(kx_0)}{x_0}, \tag{30}$$

and the boundary condition $\bar{\xi}(\pm a) = \pm\delta$ requires

$$\delta = \frac{c_1 \sinh(ka) + c_2 \cosh(ka)}{a}. \tag{31}$$

The independent solution $\cosh(kx_0)/x_0$ in equation (30) diverges at $x_0 = 0$. If we insist that the linear solution is valid everywhere, then we must set $c_2 = 0$; the boundary condition (31) then determines the coefficient $c_1 = a\delta/\sinh(ka)$. However, this solution is not physically tenable. Because $\lim_{x_0\to 0} \sinh(k|x_0|)/x_0 = k$, the geometry of the flux surfaces is approximately given by $x \simeq x_0 + (ka\delta/\sinh(ka))\cos(ky)$ in the vicinity of $x_0 = 0$. Hence, the flux surfaces with $|x_0| \lesssim ka\delta/\sinh(ka)$ overlap, causing a condition that is physically not permitted. We conclude that the linear solution is not valid within an inner region with $|x_0| \lesssim O(ka\delta/\sinh(ka))$ and a nonlinear solution must be sought.

2.3. Inner-layer solution

A general nonlinear solution for the inner layer near a resonant surface was first developed by Rosenbluth, Dagazian, and Rutherford (RDR) for the bifurcated equilibrium after an ideal internal kink instability [23]. The RDR solution was later adapted to the HKT problem with $p = 0$ [17, 18]. Here, we generalize previous approaches to incorporate pressure-gradient effects.

Because the inner region is a thin layer, we assume the conditions $|\partial x/\partial y| \ll 1$ and $|\partial/\partial y| \ll |\partial/\partial x_0|$ are satisfied. Under these assumptions, the dominant balance of the GS equation (23) is given by

$$\frac{\partial}{\partial x_0}\left(\frac{B_y^2}{2} + P(x_0)\right) = 0. \tag{32}$$

Integrating equation (32) yields

$$B_y = \frac{1}{\partial x/\partial x_0}\frac{\mathrm{d}\psi}{\mathrm{d}x_0} = \mathrm{sgn}\left(\frac{\mathrm{d}\psi}{\mathrm{d}x_0}\right)\sqrt{f(x_0) + g(y)}, \tag{33}$$

where

$$f(x_0) = -2P(x_0) + \mathrm{const} \tag{34}$$

and $g(y)$ is an arbitrary function that will be determined later by asymptotic matching of the inner-layer solution to the outer-region solution. The $\mathrm{sgn}(\mathrm{d}\psi/\mathrm{d}x_0)$ factor comes from the requirement that $\partial x/\partial x_0 > 0$ must be satisfied to avoid overlapping flux surfaces. Without loss of generality, we are free to set $f(0) = 0$, and the tangential discontinuity of B_y at $x_0 = 0$ is then given by

$$B_y|_{0^\pm} = \pm\sqrt{g(y)}. \tag{35}$$

This tangential discontinuity corresponds to a Dirac δ-function singularity in the current density.

Using the flux function $\psi = x_0^2/2$ for the HKT problem and integrating equation (33) again yields the inner-layer solution of RDR

$$x_{\mathrm{RDR}}(x_0, y) = h(y) + \int_0^{x_0} \frac{|x'|}{\sqrt{f(x') + g(y)}}\mathrm{d}x', \tag{36}$$

where the function $h(y)$, which describes the geometry of the resonant surface, is yet to be determined.

2.4. Incompressibility constraint

The functions $f(x_0)$ and $g(y)$ are not independent, but are implicitly related through equation (34) as we will see below. First, we determine B_z and p in the inner layer by substituting $x_{\mathrm{RDR}}(x_0, y)$ for $x(x_0, y)$ in equations (18) and (20). Then, applying the obtained B_z and p in equation (34), the resulting relation

$$\begin{aligned} f(x_0) = &-\frac{B_{z0}(x_0)^2}{|x_0|^2}\left\langle (f(x_0) + g(y))^{-1/2}\right\rangle^{-2} \\ &- 2\frac{p_0(x_0)}{|x_0|^\gamma}\left\langle (f(x_0) + g(y))^{-1/2}\right\rangle^{-\gamma} + \mathrm{const} \end{aligned} \tag{37}$$

gives a relation between $f(x_0)$ and $g(y)$.

We now show that equation (37) is approximately equivalent to the incompressible constraint in the strong-guide-field limit with $B_p^2 \sim p \ll B_z^2$. From equation (37), the differentials $\mathrm{d}f$ and $\mathrm{d}x_0$ are related by

$$\begin{aligned} \mathrm{d}f = &\frac{2{B_{z0}}^2}{|x_0|^2}\left\langle (f+g)^{-1/2}\right\rangle^{-2} \\ &\times\left(\frac{1}{x_0}\mathrm{d}x_0 - \frac{1}{2}\left\langle (f+g)^{-1/2}\right\rangle^{-1}\left\langle (f+g)^{-3/2}\right\rangle \mathrm{d}f\right) \\ &+ \frac{2\left(p_0' + B_{y0}B_{y0}'\right)}{|x_0|^2}\left\langle (f+g)^{-1/2}\right\rangle^{-2}\mathrm{d}x_0 \\ &+ \left(2\gamma\frac{p_0}{|x_0|^\gamma x_0} - 2\frac{p_0'}{|x_0|^\gamma}\right)\left\langle (f+g)^{-1/2}\right\rangle^{-\gamma}\mathrm{d}x_0 \\ &- \gamma\frac{p_0}{|x_0|^\gamma}\left\langle (f+g)^{-1/2}\right\rangle^{-\gamma-1}\left\langle (f+g)^{-3/2}\right\rangle \mathrm{d}f, \end{aligned} \tag{38}$$

where we have used the relation $p_0' + B_{z0}B_{z0}' + B_{y0}B_{y0}' = 0$ to eliminate B_{z0}'. In the strong-guide-field limit, the first term in the right-hand side of equation (38) is the dominant term. As the leading order approximation, we may ignore other terms in the equation, resulting in the relation

$$\frac{1}{x_0}\mathrm{d}x_0 \simeq \frac{1}{2}\left\langle (f+g)^{-1/2}\right\rangle^{-1}\left\langle (f+g)^{-3/2}\right\rangle \mathrm{d}f. \tag{39}$$

Integrating equation (39) yields

$$|x_0| \simeq C\left\langle (f+g)^{-1/2}\right\rangle^{-1}, \tag{40}$$

where C is a constant. Finally, we apply equation (40) in equation (36) and obtain

$$\left\langle \frac{\partial x_{\mathrm{RDR}}}{\partial x_0} \right\rangle = |x_0| \left\langle (f+g)^{-1/2} \right\rangle \simeq C. \tag{41}$$

Equation (41) has a simple physical meaning: the plasma in the inner layer is uniformly compressed or expanded, and the constant C is the compression ratio. Because the inner-layer solution is to be matched to the outer-region solution and the latter is not compressive (up to the linear approximation), the compression ratio must assume the value $C=1$; that is, the plasma approximately satisfies the incompressibility constraint. It should be noted, however, that the incompressibility constraint is not valid if the boundary perturbation has an $m=0$ Fourier component. In this case, the constant C needs to be determined by the asymptotic matching as well.

2.5. Asymptotic matching

The inner-layer solution must be asymptotically matched with the outer-region solution to have a complete solution. For simplicity, we will assume the strong-guide-field limit and replace the relation (37) by the incompressibility constraint

$$|x_0| = \left\langle (f+g)^{-1/2} \right\rangle^{-1}. \tag{42}$$

In this limit, to the leading order approximation, the effect of the pressure gradient on the geometry of flux surfaces is negligible. Moreover, because the pressure gradient also does not affect the outer-region solution, the asymptotic matching procedure, which we will outline below, is identical to that for the case with $p=0$ [17].

The outer-region solution is expressed in terms of the displacements ξ of flux surfaces. Therefore, to facilitate the matching, we express the flux surface displacement of the inner-layer solution as

$$\xi(x_0,y) = h(y) + \int_0^{x_0} \left(\frac{|x'|}{\sqrt{f(x')+g(y)}} - 1 \right) \mathrm{d}x' \tag{43}$$

and examine its asymptotic behavior as $x_0 \to \pm\infty$.

From the incompressibility constraint (42), we can infer that $f \to x_0^2$ as $x_0 \to \pm\infty$. Hence, in the asymptotic limit of $x_0 \to \pm\infty$ we can split the integral in equation (43) into two parts, yielding

$$\begin{aligned}\xi(x_0,y) &\simeq h(y) + \mathrm{sgn}(x_0) \int_0^{\infty} \left(\frac{x'}{\sqrt{f(x')+g(y)}} - 1 \right) \mathrm{d}x' \\ &\quad - \mathrm{sgn}(x_0) \int_{|x_0|}^{\infty} \left(\frac{x'}{\sqrt{x'^2+g(y)}} - 1 \right) \mathrm{d}x' \\ &\simeq h(y) + \mathrm{sgn}(x_0) \left[\int_0^{\infty} \left(\frac{x'}{\sqrt{f(x')+g(y)}} - 1 \right) \mathrm{d}x' \right] \\ &\quad + \frac{1}{2}\frac{g(y)}{x_0}. \end{aligned} \tag{44}$$

This asymptotic behavior of the inner-layer solution as $x_0 \to \pm\infty$ should match the behavior of the outer-region solution in the limit of $x_0 \to 0^{\pm}$, which is

$$\xi(x_0,y) \simeq \left[\mathrm{sgn}(x_0) c_1 k + \frac{c_2}{x_0} \right] \cos(ky). \tag{45}$$

Matching equations (44) and (45) yields $h(y)=0$ and the following two conditions:

$$\int_0^{\infty} \left(\frac{x'}{\sqrt{f(x')+g(y)}} - 1 \right) \mathrm{d}x' = c_1 k \cos(ky) \tag{46}$$

and

$$\frac{1}{2}\frac{g(y)}{x_0} \leftrightarrow \frac{c_2}{x_0}\cos(ky). \tag{47}$$

Here, we use the notation $\leftrightarrow$ in the second condition because, as we will see later, equation (47) cannot be matched exactly.

The matching condition (46) gives an integral equation to determine the function $g(y)$ as follows: by eliminating x' in favor of f using the incompressibility constraint (42) in equation (46), we obtain

$$\begin{aligned}&\int_0^{\infty} \left((f+g)^{-1/2} - \left\langle (f+g)^{-1/2} \right\rangle \right) \left\langle (f+g)^{-1/2} \right\rangle^{-3} \\ &\quad \times \left\langle (f+g)^{-3/2} \right\rangle \mathrm{d}f = c_1 k \cos(ky). \end{aligned} \tag{48}$$

However, analytically solving this equation to obtain $g(y)$ is a daunting task. By studying the behavior of $g(y)$ around $y=0$ and $y=\pi/k$, RDR suggested a function form $g(y) \propto \sin^8(ky/2)$ as an approximate solution. This suggestion was confirmed by Loizu and Helander with a numerical solution of the integral equation [24]. Moreover, by fitting the function form with the numerical solution, they also determined the coefficient in front, yielding

$$g(y) \simeq \frac{4c_1^2k^2}{3}\sin^8(ky/2). \tag{49}$$

Next, for the matching condition (47), it is clear that $g(y)$ cannot be matched with $\cos(ky)$ exactly. Following RDR, we expand $g(y)$ as a Fourier series

$$g(y) = \sum_{m=0}^{\infty} \Gamma_m \cos(mky) \tag{50}$$

and only match the $m=1$ term; that gives

$$c_2 = -\frac{7c_1^2k^2}{24}. \tag{51}$$

Finally, we use the relation (51) to eliminate c_2 in the boundary condition (31), yielding an equation for c_1:

$$7k^2\cosh(k/2)c_1^2 - 24\sinh(k/2)c_1 + 12\delta = 0. \tag{52}$$

The solution is

$$c_1 = \frac{12\sinh(ka) - \sqrt{144\sinh^2(ka) - 84\delta k^2\cosh(ka)}}{7k^2\cosh(ka)}. \quad (53)$$

Here, the sign for the square root in equation (53) is chosen such that $c_1 \simeq \delta/2\sinh(k/2)$ in the limit of a small perturbation.

Now, we have obtained c_1, c_2, $h(y)$, and $g(y)$. We can then solve equation (42) to obtain $f(x_0)$, which completes the necessary information to calculate the RDR solution, equation (36). Solving $f(x_0)$ from equation (42) in general requires a numerical treatment. However, the leading order behavior of $f(x_0)$ in the limit of $|x_0| \to 0$ can be obtained analytically as [18]

$$f(x_0) \simeq (c_f|x_0|)^{8/3}, \quad (54)$$

where the coefficient c_f can be expressed in terms of the gamma function Γ [25] as

$$c_f \equiv \frac{2(3/4)^{1/8}}{\pi^{3/2}}\Gamma(3/8)\Gamma(9/8)\,(c_1 k)^{-1/4} \simeq 0.7735\,(c_1 k)^{-1/4}. \quad (55)$$

2.6. Pressure-gradient-driven current singularity

Our analysis thus far has shown that the effect of pressure gradient on the geometry of flux surfaces is negligible. We are now in a position to discuss the effect of the pressure gradient on the current density distribution. We are primarily interested in the current density near the resonant surface, i.e. the inner-layer solution.

In the strong-guide-field limit, the plasma is approximately incompressible, therefore, from equations (18) and (20) we have $p(x_0) \simeq p_0(x_0)$ and $B_z(x_0) \simeq B_{z0}(x_0)$ as the leading order approximation. To calculate the current density requires $B_z'(x_0)$, but we cannot simply assume $B_z'(x_0) \simeq B_{z0}'(x_0)$ for the following reason: when the guide field is strong, both $B_z(x_0)$ and $B_{z0}(x_0)$ are close to constant, with different small variations to account for the force balance under different conditions, and these differing small variations give rise to different derivatives for the two fields. To obtain an approximation for $B_z'(x_0)$, we take the derivative of equation (34) with respect to x_0, yielding

$$\frac{\mathrm{d}f}{\mathrm{d}x_0} = -2B_zB_z' - 2p' \simeq -2B_{z0}B_z' - 2p_0'. \quad (56)$$

Hence,

$$B_z' \simeq \frac{-p_0'}{B_{z0}} - \frac{1}{2B_{z0}}\frac{\mathrm{d}f}{\mathrm{d}x_0}. \quad (57)$$

Using equation (57) in equation (22) we can obtain the poloidal current density

$$\begin{aligned}\boldsymbol{J}_p &= \frac{\mathrm{d}B_z}{\mathrm{d}\psi}\nabla\psi\times\hat{\boldsymbol{z}} \\ &= -\left(\frac{\mathrm{d}\psi}{\mathrm{d}x_0}\right)^{-1}\frac{\mathrm{d}B_z}{\mathrm{d}x_0}\boldsymbol{B}_p \simeq \frac{1}{x_0}\left[p_0' + \frac{1}{2}\frac{\mathrm{d}f}{\mathrm{d}x_0}\right]\frac{\boldsymbol{B}_p}{B_{z0}}. \end{aligned} \quad (58)$$

In the vicinity of $x_0 = 0$, $f \sim |x_0|^{8/3}$ and $\mathrm{d}f/\mathrm{d}x_0 \sim |x_0|^{5/3}$. Assuming $p_0' \neq 0$, the pressure gradient term dominates and the poloidal current density diverges as $J_p \sim p_0'/x_0$.

Next, we calculate the out-of-plane current density $J_z = \hat{\boldsymbol{z}}\cdot\nabla\times\boldsymbol{B}_p$. The dominant component of $\boldsymbol{B}_p$ is $B_y \simeq \mathrm{sgn}(x_0)\sqrt{f(x_0)+g(y)}$. Therefore, the out-of-plane current density

$$\begin{aligned} J_z &\simeq \left(\frac{\partial B_y}{\partial x}\right)_y = \left(\frac{\partial x}{\partial x_0}\right)^{-1}\frac{\partial B_y}{\partial x_0} \simeq \frac{\sqrt{f+g}}{|x_0|}\frac{\mathrm{sgn}(x_0)}{2\sqrt{f+g}}\frac{\mathrm{d}f}{\mathrm{d}x_0} \\ &= \frac{1}{2x_0}\frac{\mathrm{d}f}{\mathrm{d}x_0}, \end{aligned} \quad (59)$$

which is not affected by the pressure. Using the asymptotic behavior (54), the leading order behavior of J_z near $x_0 = 0$ is

$$J_z \simeq \frac{4}{3}c_f^{8/3}|x_0|^{2/3}. \quad (60)$$

Hence, the out-of-plane component $J_z \to 0$ as $x_0 \to 0$.

Now we put our results in the context of the conventional treatment of the Pfirsch–Schlüter current density. For a solution to the GS equation, the perpendicular component of the current density is

$$\begin{aligned}\boldsymbol{J}_\perp &= \frac{\boldsymbol{B}\times\nabla p}{B^2} = \frac{1}{B^2}\left(B_z\hat{\boldsymbol{z}} + \hat{\boldsymbol{z}}\times\nabla\psi\right)\times\nabla p \\ &= \frac{1}{B^2}\frac{\mathrm{d}p}{\mathrm{d}\psi}\left(B_z\boldsymbol{B}_p - B_p^2\hat{\boldsymbol{z}}\right), \end{aligned} \quad (61)$$

and the divergence of $\boldsymbol{J}_\perp$ is

$$\begin{aligned}\nabla\cdot\boldsymbol{J}_\perp &= (\boldsymbol{B}\times\nabla p)\cdot\nabla\frac{1}{B^2} = \frac{\mathrm{d}p}{\mathrm{d}\psi}\left(B_z\boldsymbol{B}_p - B_p^2\hat{\boldsymbol{z}}\right)\cdot\nabla\frac{1}{B^2} \\ &= \boldsymbol{B}_p\cdot\nabla\left(\frac{B_z}{B^2}\frac{\mathrm{d}p}{\mathrm{d}\psi}\right). \end{aligned} \quad (62)$$

Here, we have used that z is the direction of symmetry and that both p and B_z are flux functions.

The parallel current density is given by

$$\begin{aligned} J_\parallel &= \frac{J_zB_z + \boldsymbol{J}_p\cdot\boldsymbol{B}_p}{B} = \frac{1}{B}\left(B_z\nabla^2\psi - \frac{\mathrm{d}B_z}{\mathrm{d}\psi}B_p^2\right) \\ &= \frac{1}{B}\left(B_z\nabla^2\psi - \frac{\mathrm{d}B_z}{\mathrm{d}\psi}\left(B^2 - B_z^2\right)\right) \\ &= -B\frac{\mathrm{d}B_z}{\mathrm{d}\psi} - \frac{B_z}{B}\frac{\mathrm{d}p}{\mathrm{d}\psi}. \end{aligned} \quad (63)$$

Here, in the last step we have applied the GS equation (11). From equations (62) and (63), we see that the magnetic differential equation (4) is indeed satisfied:

$$\boldsymbol{B}\cdot\nabla\frac{J_\parallel}{B} = -\boldsymbol{B}_p\cdot\nabla\left(\frac{B_z}{B^2}\frac{\mathrm{d}p}{\mathrm{d}\psi}\right) = -\nabla\cdot\boldsymbol{J}_\perp. \quad (64)$$

For the HKT problem, the parallel and the perpendicular components of the current density can be obtained from equations (61) and (63) as

$$J_\parallel = -\frac{B}{x_0}\frac{\mathrm{d}B_z}{\mathrm{d}x_0} - \frac{B_z}{x_0B}\frac{\mathrm{d}p}{\mathrm{d}x_0} \simeq \frac{B}{B_z}\left(\frac{1}{2x_0}\frac{\mathrm{d}f}{\mathrm{d}x_0} + \frac{p'}{x_0}\frac{B_p^2}{B^2}\right) \quad (65)$$

and

$$\boldsymbol{J}_\perp = \frac{p'}{x_0 B^2}\left(B_z \boldsymbol{B}_p - B_p^2 \hat{\boldsymbol{z}}\right). \tag{66}$$

Alternatively, we can also obtain $J_\parallel$ and $\boldsymbol{J}_\perp$ from equations (58) and (59) by making appropriate projections. Note that $J_\parallel \propto B_p^2/B^2$ and $J_\perp \propto B_p/B$; therefore, in the strong-guide-field limit the perpendicular component $J_\perp$ dominates.

Equations (65) and (66) show that the Pfirsch–Schlüter current density $J_\parallel$ and the diamagnetic current density $\boldsymbol{J}_\perp$ both diverge as p'/x_0. If we assume that the system size along the z direction is the same as the size L along the y direction, the equivalent 'rotational' transform is given by

$$\iota(x_0) = \frac{B_{y0}}{B_{z0}} = \frac{x_0}{B_{z0}}. \tag{67}$$

Now, if we use the symbol x to represent the rotational transform ι for the time being, the Pfirsch–Schlüter current density does have a $1/x$-type singularity; however, the underlying reason for its divergence is not the one commonly assumed.

In the conventional picture, the $1/x$-type singularity arises because the magnetic differential operator $\boldsymbol{B}\cdot\nabla$ is thought to become non-invertible at rational surfaces, as suggested by the expressions (4) and (8) using a straight-field line coordinate system. It is commonly assumed that $\nabla\cdot\boldsymbol{J}_\perp$ and the straight-field-line coordinate system are well-behaved; therefore, the $1/x$-type singularity follows from equation (9). In contrast, our results show that the diamagnetic current density $\boldsymbol{J}_\perp$ diverges as $\sim p'/x_0$ and likewise, from equation (62), that $\nabla\cdot\boldsymbol{J}_\perp$ diverges as $\sim p'/x_0$ as well. A crucial point is that because of the formation of the Dirac δ-function current singularity, the poloidal magnetic field $\boldsymbol{B}_p$ does not go to zero as at the resonant surface; instead, $\boldsymbol{B}_p \to \pm\sqrt{g(y)}\hat{\boldsymbol{y}}$ as $x_0 \to \pm 0$. Consequently, the magnetic differential operator $\boldsymbol{B}\cdot\nabla$ is invertible, and the magnetic differential equation (4) implies that the parallel current density $J_\parallel$ diverges in the same way as $\nabla\cdot\boldsymbol{J}_\perp$.[5]

How do we reconcile the fact that the operator $\boldsymbol{B}\cdot\nabla$ is invertible at the resonant surface with its non-invertible appearance in a straight-field-line coordinate system? To answer this question, it is instructive to construct such a coordinate system. Because the initial magnetic field lines are straight, the Cartesian coordinates are a straight-field-line coordinate system. Now, if we take a Lagrangian perspective by describing the final state in terms of the mapping from the initial positions $\boldsymbol{x}_0 = (x_0, y_0, z_0)$ of fluid elements to their final positions $\boldsymbol{x} = (x, y, z)$, the initial coordinates (x_0, y_0, z_0) are also a straight-field-line coordinate system for the final state due to the ideal MHD frozen-in constraint. In the Lagrangian perspective, the magnetic field at $\boldsymbol{x}$ is determined by the initial magnetic field $\boldsymbol{B}_0$ at $\boldsymbol{x}_0$ and the mapping $\boldsymbol{x}(\boldsymbol{x}_0)$ via the relation [20, 26]

$$\boldsymbol{B} = \mathcal{J}^{-1}\boldsymbol{B}_0\cdot\frac{\partial\boldsymbol{x}}{\partial\boldsymbol{x}_0}, \tag{68}$$

where $\mathcal{J} = \det(\partial\boldsymbol{x}/\partial\boldsymbol{x}_0)$ is the Jacobian of the mapping.

Although our GS formulation is not fully Lagrangian, we can reconstruct the Lagrangian mapping of fluid elements from the initial to the final state once the solution is obtained. In this 2D problem, the fluid motion is limited to an x–y plane. As a result, the z coordinates of the initial and final states are identical, $z = z_0$. In an x–y plane, for each fluid element labeled by (x_0, y) in the final state, we need to find its initial position (x_0, y_0). This 'inverse' Lagrangian mapping can be expressed as a function $y_0(x_0, y)$. From the conservation of magnetic flux through an infinitesimal fluid element

$$B_{z0}(x_0)\,dx_0\left[\frac{\partial y_0}{\partial y}\mathrm{d}y\right] = B_z(x_0)\left[\frac{\partial x}{\partial x_0}\mathrm{d}x_0\right]\mathrm{d}y \tag{69}$$

and using equation (18) to relate B_{z0} and B_z, we can calculate

$$\frac{\partial y_0}{\partial y} = \frac{\partial x/\partial x_0}{\langle\partial x/\partial x_0\rangle} \tag{70}$$

and integrate it along each constant-x_0 contour to obtain $y_0(x_0, y)$. Using the RDR solution (36) in equation (70) yields

$$\frac{\partial y_0}{\partial y} = \frac{|x_0|}{\sqrt{f(x_0)+g(y)}}. \tag{71}$$

In the limit of $x_0 \to 0$, $\partial y_0/\partial y \to 0$ everywhere except at $y = 0$ and $y = L$, where $\partial y_0/\partial y$ diverges as $\sim|x_0|^{-1/3}$. Therefore, the straight-field-line coordinate system (x_0, y_0, z_0) becomes ill-behaved at the resonant surface which explains why the invertible operator $\boldsymbol{B}\cdot\nabla$ appears to be non-invertible in such a coordinate system. Figure 2 shows a constant-z_0 slice of the straight-field-line coordinate (x_0, y_0, z_0) for the HKT problem with $L = 2\pi$, $a = 0.5$, and $\delta = 0.1$, where the solid lines are constant-x_0 or constant-y_0 coordinate curves. The singular nature of the coordinate system at the resonant surface is evident, as all the constant-y_0 coordinate curves converge toward $y = 0$ or $y = L$.

The critical question now is: does the $1/x$-type current singularity lead to an infinite current? Fortunately, the answer is no, and the reason can be attributed to the Dirac δ-function singularity that simultaneously appears at the resonant surface. The finite tangential discontinuity $[\![B_y]\!]_{x_0=0} = 2\sqrt{g(y)}$, where $[\![\cdot]\!]$ denotes the jump across an interface, arises from a continuous initial magnetic field by squeezing the space between flux surfaces [16]. We can infer from the RDR solution (36) that,

[5] Strictly speaking, it may be more appropriate to describe the operator $\boldsymbol{B}\cdot\nabla$ as conditionally invertible at $x_0 = \pm 0$. Because the function g goes to zero at $y = 0$ and L, the equation $\pm\sqrt{g(y)}\mathrm{d}\varrho/\mathrm{d}y = \varsigma$ is solvable only when ς approaches zero sufficiently fast as y approaches 0 and L such that the function $\varsigma/\sqrt{g}$ is integrable. This condition is satisfied for $-\nabla\cdot\boldsymbol{J}_\perp$ on the right-hand side of the magnetic differential equation (4).

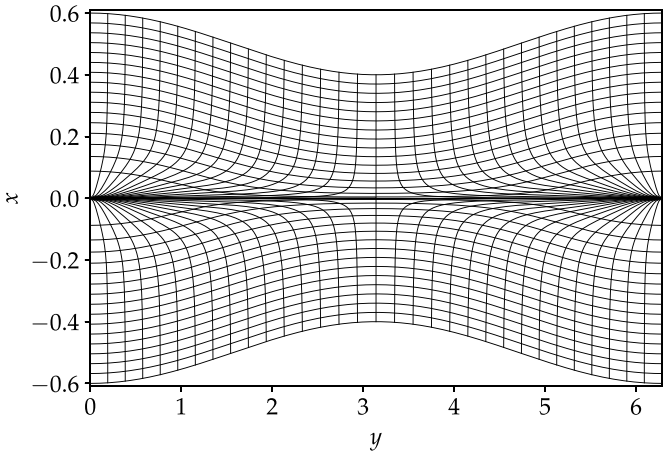

Figure 2. A straight-field-line coordinate system for the HKT problem with $L = 2\pi$, $a = 0.5$, and $\delta = 0.1$. The coordinate system becomes ill-behaved at the resonant surface.

for flux surfaces sufficiently close to the resonant surface such that the condition

$$f(x_0) \ll g(y) \tag{72}$$

is satisfied, the mapping from the flux surface label x_0 to the physical distance s is quadratic:

$$s = |x(x_0, y)| \simeq \frac{x_0^2}{\sqrt{g(y)}}. \tag{73}$$

Because $f(x_0) \sim |x_0|^{8/3}$ and $g(y) \simeq \left(4c_1^2k^2/3\right)\sin^8(ky/2)$, where $k = 2\pi/L$, the condition (72) eventually will be satisfied with a sufficiently small x_0 for all y except at $y = 0$ and $y = L$. As such, the mapping eventually becomes quadratic, $s \sim x_0^2$, although the transition to the quadratic mapping will occur at different x_0 for different y. Because of the quadratic mapping, the poloidal current density $J_p \sim 1/x_0$ becomes $J_p \sim 1/\sqrt{s}$. And since $\int_0^s \mathrm{d}s'/\sqrt{s'}$ is integrable, the total current does not diverge.

What about at $y = 0$ and $y = L$ where the mapping is not quadratic? Because $g = 0$ at those locations and $f \sim |x_0|^{8/3}$, equation (58) gives $J_p \sim |x_0|^{1/3}$, which does not diverge. Moreover, to compensate for the strong squeezing of the quadratic mapping, the flux surfaces in the downstream regions near $y = 0$ and $y = L$ have to bulge out. Consequently, the scaling at $y = 0$ and $y = L$ becomes $s \sim |x_0|^{2/3}$; see [18].

Intuitively, the $J \sim 1/\sqrt{s}$ scaling can be understood as follows. The quadratic mapping $s \sim x_0^2$ causes a steepening of the pressure gradient:

$$\frac{\partial p}{\partial x} = \left(\frac{\partial x}{\partial x_0}\right)^{-1}\frac{\partial p}{\partial x_0} \sim \frac{1}{x_0}\frac{\partial p}{\partial x_0} \sim \frac{1}{\sqrt{s}}\frac{\partial p}{\partial x_0}. \tag{74}$$

Because the pressure gradient is balanced by the $\boldsymbol{J}\times\boldsymbol{B}$ force for an MHD equilibrium, the perpendicular current density $J_\perp \sim |\nabla p| \sim 1/\sqrt{s}$, and $\nabla\cdot\boldsymbol{J}_\perp$ diverges in the same manner. Finally, the parallel current density satisfies the magnetic differential equation (4), and the operator $\boldsymbol{B}\cdot\nabla$ is invertible, therefore, $J_\parallel \sim 1/\sqrt{s}$ as well.

3. Numerical verification of the analytic solutions

We now compare the analytic solutions in section 2 with numerical solutions using a GS solver. The GS solver has been extensively tested, showing good agreement with the solutions of a fully Lagrangian solver [16] and the SPEC code [18] for the HKT problem with $p = 0$. Here, we consider an initial equilibrium with a linear pressure profile

$$p_0 = \bar{p_0} + rx_0 \tag{75}$$

and a magnetic field

$$\boldsymbol{B}_0 = x_0\hat{\boldsymbol{y}} + \sqrt{B_0^2 - 2rx_0 - x_0^2}\hat{\boldsymbol{z}}. \tag{76}$$

The parameters in the following numerical calculations are as follows: the domain sizes $a = 1/2$ and $L = 2\pi$; the guide field $B_0 = 10$; the mean pressure $\bar{p_0} = 1$; the pressure gradient $r = 1$; the perturbation amplitude $\delta = 0.1$; the adiabatic index $\gamma = 5/3$.

In our previous studies, we assumed a mirror symmetry across the mid-plane and only solved the GS equation in half of the domain with $x_0 \geqslant 0$. In this study, because of the asymmetric pressure profile across the resonant surface, we cannot impose mirror symmetry. We divide the domain into two regions separated by the flux surface labeled by $x_0 = 0$ and solve the GS equation in each region by a descent method. Simultaneously with the iteration in both regions, the $x_0 = 0$ flux surface is allowed to move until the force-balance condition $[\![B^2/2 + p]\!] = 0$ is satisfied.

Panel (a) of figure 3 shows a numerical solution of the B_y component in the entire domain. Panels (b)–(d) show a few selected one-dimensional (1D) cuts of the numerical

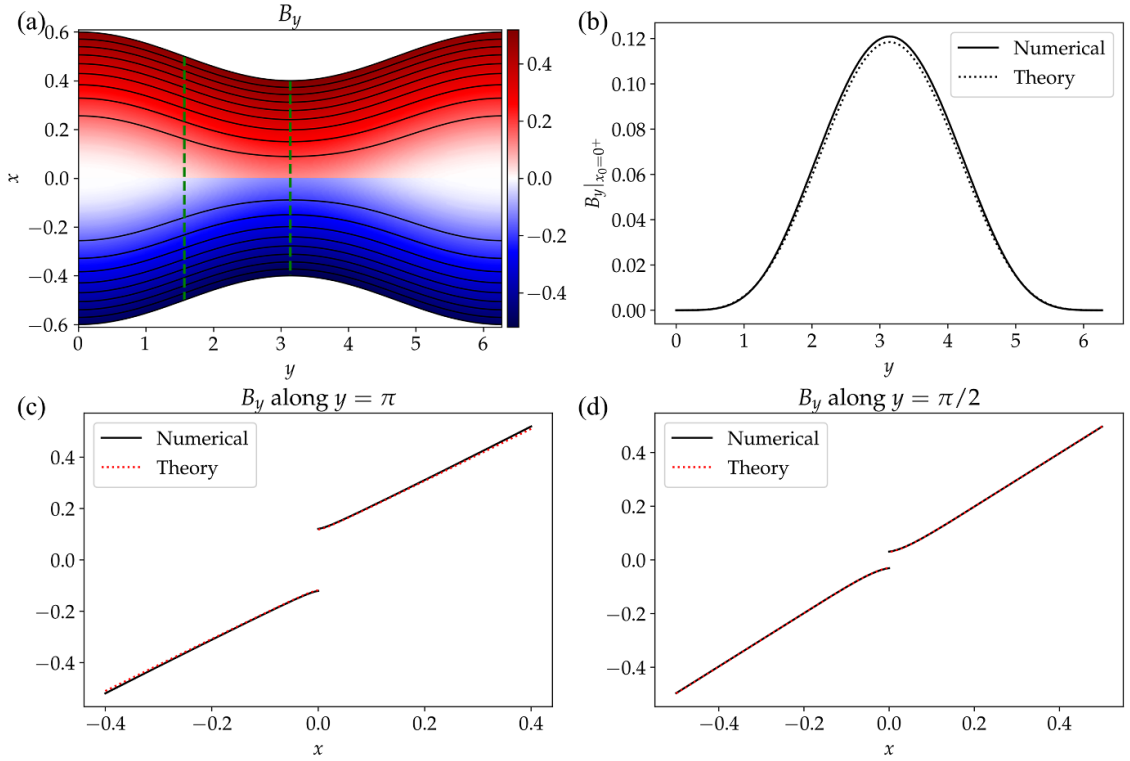

Figure 3. Magnetic field component B_y (a) in the entire domain; (b) along $x_0 = 0^+$; (c) along $y = \pi$; (d) along $y = \pi/2$. Black solid lines in panel (a) are flux surfaces, and vertical dashed lines indicate the locations of the one-dimensional cuts of panels (c) and (d). The black solid lines in panels (b)–(d) are numerical results, and the red dotted lines are the predictions of the analytic theory.

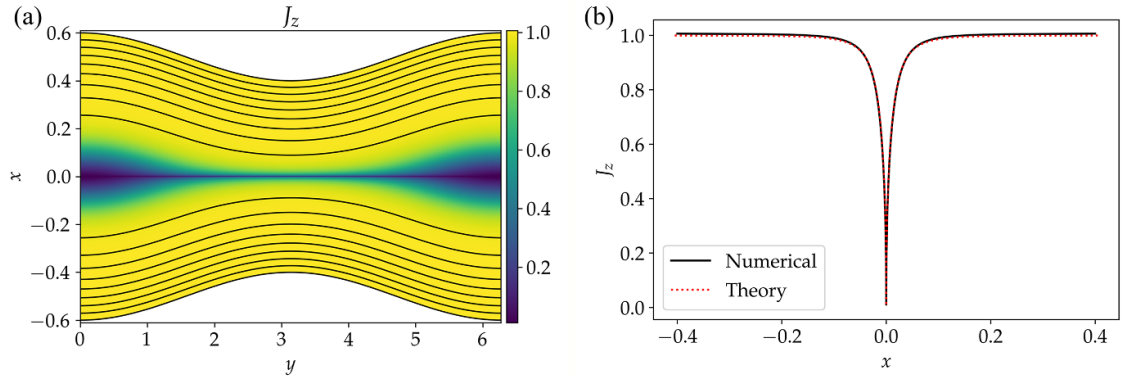

Figure 4. (a) A numerical solution of J_z in the entire domain; (b) 1D cuts along $y = \pi$ in panel (a). The black solid line in panel (b) is the numerical solution, and the red dotted line is the prediction of the analytic theory.

solution, together with the corresponding analytical solution (33). The analytical and numerical solutions are in good agreement. The magnetic field is discontinuous across the resonant surface, corresponding to a Dirac δ-function current singularity.

Figure 4 compares the numerical solution of the J_z component with the theoretical prediction using equation (59). Here, $J_z \to 0$ at the resonant surface, as the theory predicts. Likewise, figure 5 shows comparisons between the numerical solutions of J_y along selected 1D cuts and the theoretical predictions using equation (58). In this figure, the horizontal axis $|x - x_r|$ is the distance between the flux surface at x and the resonant surface at x_r. As predicted by the theory, J_y diverges as $|x - x_r|^{-1/2}$ near the resonant surface.

Finally, figure 6 shows a numerical solution for the pressure p in the entire domain and along selected 1D cuts. Here, the steepening of the pressure gradient due to the squeezing of flux surfaces near the resonant surface is evident. Examining the solutions near the resonant surface indicates that the $\partial p/\partial x \sim |x - x_r|^{-1/2}$, as expected from our analysis.

We remark that although the analytic theory is derived under the strong-guide-field limit, we find that the theoretical predictions remain close to numerical results even for a moderate guide field such as $B_0 = 2$.

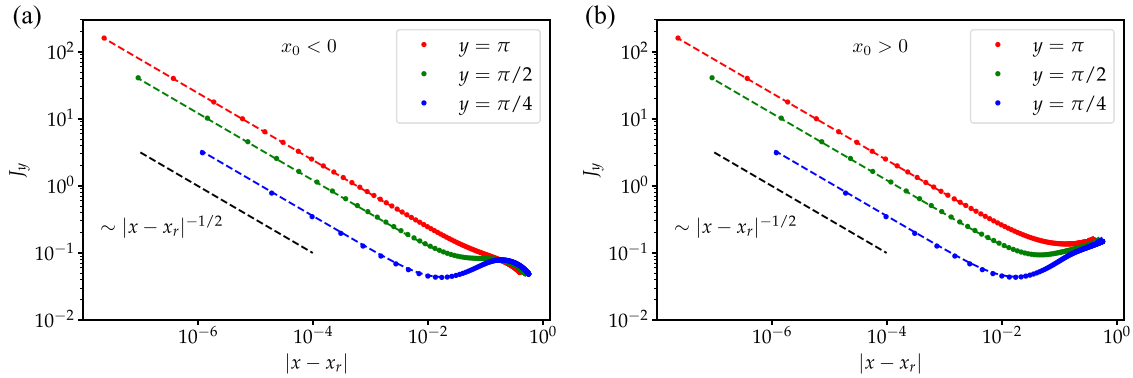

Figure 5. Comparisons between the numerical solutions of J_y and the theoretical predictions along a few 1D cuts. Here, the solid dots represent the numerical solutions and the dashed lines are theoretical predictions. Panel (a) shows the region with $x_0 < 0$ and panel (b) shows the region with $x_0 > 0$. Here, the horizontal axis $|x - x_r|$ is the distance between the flux surface at x and the resonant surface at x_r. As predicted by the theory, J_y diverges as $|x - x_r|^{-1/2}$ near the resonant surface.

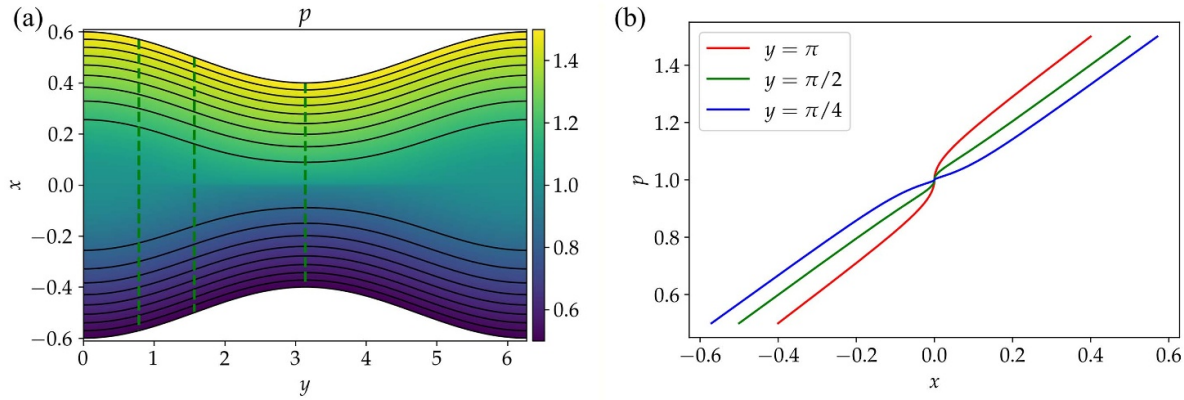

Figure 6. (a) A numerical solution of the pressure p in the entire domain; (b) 1D cuts along the dashed lines in panel (a).

4. Discussions and conclusion

In summary, we have derived an analytic theory for the pressure-gradient-driven current singularity near the resonant surface of the ideal HKT problem and have validated the theory with numerical solutions. Our key finding is that although the current density diverges as $J \sim 1/\Delta\iota$, where $\Delta\iota$ is the difference of the rotational transition relative to the resonant surface, this singularity does not lead to a divergent total current. This is because the distance s between the resonant surface and the adjacent flux surface is not proportional to $\Delta\iota$. Due to the formation of a Dirac δ-function current sheet at the resonant surface, the neighboring flux surfaces are strongly packed, and the distance $s \sim (\Delta\iota)^2$. Consequently, the current density $J \sim 1/\sqrt{s}$, which is integrable and the total current is finite.

Our analysis also finds that the Pfirsh–Schlüter current density $J_\parallel$ and the diamagnetic current density $\boldsymbol{J}_\perp$ both diverge as $1/\sqrt{s}$, where the diamagnetic current density is the dominant component. The diamagnetic current density diverges because the strong packing of flux surfaces near the resonant surface causes a steepening of the pressure gradient; therefore, $\boldsymbol{J}_\perp \sim \mathrm{d}p/\mathrm{d}s \sim 1/\sqrt{s}$. Furthermore, solving the magnetic differential equation (4) yields the parallel current density $J_\parallel$ diverging in the same manner as the perpendicular component $\boldsymbol{J}_\perp$. Notably, contrary to the conventional wisdom that the pressure needs to flatten at rational surfaces to have an integrable current density, here we show that the current singularity remains integrable despite a steepening of the pressure gradient.

Our analysis assumes that the initial pressure gradient $\mathrm{d}p/\mathrm{d}x_0$ does not diverge and is non-vanishing at $x_0 = 0$. More generally, we may consider an initial condition with $J_p \sim \mathrm{d}p/\mathrm{d}x_0 \sim |x_0|^\alpha$, where $\alpha > -1$ such that the current density is integrable. After the boundary perturbation, the current density $J \sim \mathrm{d}p/\mathrm{d}s \sim s^{(\alpha-1)/2}$. Because of the power index $(\alpha - 1)/2 > -1$ if $\alpha > -1$, the current density is integrable. Furthermore, we may consider an initial magnetic field $B_{y0} \sim \mathrm{sgn}\,(x_0)\,|x_0|^\nu$. After the boundary perturbation, the formation of a Dirac δ-function current sheet requires the distance between the flux surfaces to scale as $s \sim |x_0|^{\nu+1}$; consequently, the current density $J \sim \mathrm{d}p/\mathrm{d}s \sim s^{(\alpha-\nu)/(\nu+1)}$, which is integrable. In all these cases, as long as the initial current density is integrable, the current density in the perturbed state is also integrable.

Although our conclusion is obtained with a simple prototype problem, a similar conclusion probably applies to more

general magnetic fields and potentially resolves the paradox of non-integrability of the Pfirsch–Schlüter current density. If that is to be the case, then a weak (i.e. non-smooth) ideal MHD equilibrium solution with a continuum of nested flux surfaces, a continuous pressure distribution with non-vanishing pressure gradients on rational surfaces, and a continuous rotational transition is not prohibited. Such an equilibrium may be pathological, to quote Grad, but nonetheless mathematically intriguing to contemplate.

Data availability statement

The data that support the findings of this study are available upon reasonable request from the authors.

Acknowledgments

We thank Dr Greg Hammett for beneficial discussion. This research was supported by the U.S. Department of Energy under Contract No. DE-AC02-09CH11466 and by a grant from the Simons Foundation/SFARI (560651, A B). Part of this work has been carried out within the framework of the EUROfusion Consortium and has received funding from the Euratom research and training programme 2014–2018 and 2019–2020 under Grant Agreement No. 633053. The views and opinions expressed herein do not necessarily reflect those of the European Commission. Y Z was sponsored by Shanghai Pujiang Program under Grant No. 21PJ1408600. Part of the numerical calculations were performed with computers at the National Energy Research Scientific Computing Center.

ORCID iDs

Yi-Min Huang https://orcid.org/0000-0002-4237-2211
Yao Zhou https://orcid.org/0000-0002-3616-2912
Stuart Hudson https://orcid.org/0000-0003-1530-2733

References

[1] Spitzer L 1958 The stellarator concept *Phys. Fluids* **1** 253
[2] Boozer A H 1998 What is a stellarator *Phys. Plasmas* **54** 1647–55
[3] Helander P 2014 Theory of plasma confinement in non-axisymmetric magnetic fields *Rep. Prog. Phys.* **77** 087001
[4] Boozer A H 2015 Stellarator design *J. Plasma Phys.* **81** 515810606
[5] Hirshman S P and Whitson J C 1983 Steepest-descent moment method for three-dimensional magnetohydrodynamic equilibria *Phys. Fluids* **26** 3553
[6] Taylor M 1994 A high performance spectral code for nonlinear MHD stability *J. Comput. Phys.* **110** 407–18
[7] Garabedian P R 2002 Three-dimensional stellarator codes *Proc. Natl Acad. Sci.* **99** 10257–9
[8] Dudt D W and Kolemen E 2020 DESC: a stellarator equilibrium solver *Phys. Plasmas* **27** 102513
[9] Cary J R and Kotschenreuther M 1985 Pressure induced islands in three-dimensional toroidal plasma *Phys. Fluids* **28** 1392
[10] Hegna C C and Bhattacharjee A 1989 Magnetic island formation in three-dimensional plasma equilibria *Phys. Fluids* B **1** 392–7
[11] Grad H 1967 Toroidal containment of a plasma *Phys. Fluids* **10** 137–54
[12] Hudson S R and Kraus B F 2017 Three-dimensional magnetohydrodynamic equilibria with continuous magnetic fields *J. Plasma Phys.* **83** 715830403
[13] Kraus B F and Hudson S R 2017 Theory and discretization of ideal magnetohydrodynamic equilibria with fractal pressure profiles *Phys. Plasmas* **24** 092519
[14] Hahm T S and Kulsrud R M 1985 Forced magnetic reconnection *Phys. Fluids* **28** 2412–8
[15] Dewar R L, Bhattacharjee A, Kulsrud R M and Wright A M 2013 Plasmoid solutions of the Hahm-Kulsrud-Taylor equilibrium model *Phys. Plasmas* **20** 082103
[16] Zhou Y, Huang Y-M, Qin H and Bhattacharjee A 2016 Formation of current singularity in a topologically constrained plasma *Phys. Rev.* E **93** 023205
[17] Zhou Y, Huang Y-M, Reiman A H, Qin H and Bhattacharjee A 2019 Magnetohydrodynamical equilibria with current singularities and continuous rotational transform *Phys. Plasmas* **26** 022103
[18] Huang Y-M, Hudson S R, Loizu J, Zhou Y and Bhattacharjee A 2022 Numerical study of δ-function current sheets arising from resonant magnetic perturbations *Phys. Plasmas* **29** 032513
[19] Huang Y-M, Bhattacharjee A and Zweibel E G 2009 Do potential fields develop current sheets under simple compression or expansion? *Astrophys. J. Lett.* **699** L144–7
[20] Zhou Y, Qin H, Burby J W and Bhattacharjee A 2014 Variational integration for ideal magnetohydrodynamics with built-in advection equations *Phys. Plasmas* **21** 102109
[21] Hudson S R, Dewar R L, Dennis G, Hole M J, McGann M, von Nessi G and Lazerson S 2012 Computation of multi-region relaxed magnetohydrodynamic equilibria *Phys. Plasmas* **19** 112502
[22] Zhou Y, Huang Y-M, Qin H and Bhattacharjee A 2018 Constructing current singularity in a 3d line-tied plasma *Astrophys. J.* **852** 3
[23] Rosenbluth M N, Dagazian R Y and Rutherford P H 1973 Nonlinear properties of the internal $m = 1$ kink instability in the cylindrical tokamak *Phys. Fluids* **16** 1894–902
[24] Loizu J and Helander P 2017 Unified nonlinear theory of spontaneous and forced helical resonant MHD states *Phys. Plasmas* **24** 040701
[25] Abramowitz M and Stegun I A (eds) 1972 *Handbook of Mathematical Functions With Formulas, Graphs and Mathematical Tables* 10th edn (Washington, D.C.: National Bureau of Standards)
[26] Newcomb W A 1962 Lagrangian and Hamiltonian methods in magnetohydrodynamics *Nucl. Fusion Suppl.* **2** 451–63 (available at: www-thphys.physics.ox.ac.uk/people/AlexanderSchekochihin/notes/PlasmaClassics/newcomb62.pdf)